Active lift inversion process of heaving wing in uniform flow by temporal change of wing kinematics

Makoto Iima*
Department of Mathematics and Life Sciences, Hiroshima University, 1-7-1, Kagamiyama Higashi-Hiroshima, Hiroshima 749-8251, Japan

Naoto Yokoyama†
Research Center for Energy Conversion System, Doshisha University, 1-3 Tatara-miyakodani, Kyotanabe 610-0394, Japan and Department of Pure and Applied Physics, Kansai University, 3-3-35 Yamate, Suita, Osaka 564-8680 Japan

Kei Senda
Graduate School of Engineering, Kyoto University, C3 Building, Kyoto Daigaku-Katsura, Nishikyo-ku, Kyoto 615-8540, Japan

(Received 13 September 2018; published 29 April 2019)

The transition of the vortex pattern and the lift generated by a heaving wing in a uniform flow was investigated numerically. As a fundamental problem constituting the insects' flight maneuverability, we studied the relationship between a temporal change in the heaving wing motion and the change in the global vortex pattern. At a Strouhal number that generates an asymmetric vortex pattern, we found that temporal angular frequency reduction causes inversion of both the global vortex pattern and the lift sign. The inversion is initiated by the transfer of the leading-edge vortex, which interferes with the vortex pattern generated at the trailing edge. Successful inversion is conditioned on the starting phase and the time interval of the frequency reduction. The details of the process during the transition are discussed.

DOI: 10.1103/PhysRevE.99.043110

I. INTRODUCTION

Animal locomotion in fluids, such as the flight of insects and the swimming of fish, is achieved by the unsteady flow driven by wings or fins. During flight, insects exploit vortex structures generated by the motion of their wings, which makes the flight mechanisms different from those of conventional fixed-wing aerodynamics. Such mechanisms include delayed stall, rotational circulation, the clap-and-fling mechanism, and wing-wake interaction [1]; several reviews are available [1–4]. When the flight (or swimming) is steady (time-periodic), the generation, transfer, merging, and dissipation of the vortex structure during one flapping cycle are periodic.

Real insects need to maneuver their flight, i.e., control their flight speed and/or direction, e.g., take-off, landing, and changing speeds of forward flight [5,6]. Consequently, their flight is unsteady (nonperiodic), and the flight mechanisms or generated vortex structures can change. For instance, butterflies fly with a sequence of several flight modes and rapid maneuvers [5], and they use a variety of flight mechanisms in successive strokes [7]. Such changes of flight mechanisms require the control of particular vortex structures via wing kinematics. Although flight maneuverability is an important aspect of flapping flight, the study of maneuverability is limited to observations [7–9] or numerical simulations [10,11] of real animals.

For flight maneuverability and stability, unsteady wing and/or body motion are required to maintain the flight, which is regarded as unstable in many studies [12–16]. The relationship between such wing and/or body motion and the related fluid dynamics has not been clarified, except for a "damping factor" highlighted in studies on maneuverability [17] and stability [18].

Despite the fundamental importance of actively exploiting vortex structures, to the best of the authors' knowledge, few studies have investigated the fluid dynamics that connects the vortex structures, including lift generation and unsteady (nonperiodic) wing kinematics. This is partly because of the nature of the unsteady flight, i.e., a strongly coupled system consisting of (1) the motion of the center of mass and the orientation of the body, (2) body and wing motion (deformation of the animal's body), and (3) the motion of the surrounding fluid, even if we omit the sensing and control parts. Clearly, the entire system is too complex to be resolved all at once. We should break up the entire problem into fundamental pieces easier to handle with, which will contribute to resolve the maneuver problem.

Here, we remark that the analysis of the coupled system comprising (2) and (3) is interesting and difficult by itself as a fluid mechanics problem because of the nonperiodicity and the strongly nonlinear nature of fluid dynamics. Flow dynamics due to nonperiodic wing motion has not been studied in detail, except for an impulsively started object as the simplest example [19–22]. In this study, we focus on the relationship between vortex patterns (and the associated hydrodynamic force) and wing kinematics, especially for the effect of nonperiodic wing motion. If the hydrodynamic force vector and the vortex structure can be controlled via wing

*iima@hiroshima-u.ac.jp
†Present address: Department of Mechanical Science and Bioengineering, Osaka University, 1-3 Machikaneyama, Toyonaka, Osaka 560-8531, Japan

motion, such wing motion will be of potential use for efficient flight or propulsion control, e.g., control without additional apparatus such as a flap or rudder. Because the description of nonperiodic wing motion requires many parameters, we consider a model with simple wing kinematics, i.e., a heaving wing in a uniform flow with the given wing kinematics, to highlight the intrinsic nature of the wing-vortex interaction, though the model of insects' flapping motion should include other kinematics such as flapping motion.

Various types of vortex patterns are generated by an oscillating wing. Several studies have investigated vortex patterns generated by a heaving wing in a uniform flow [23–30]. In particular, wake deflection is an asymmetric vortex pattern that is ubiquitous when both the Strouhal number and the heaving amplitude are large. In this case, the sign of the average lift depends on the direction of the wake. Wake deflection has been experimentally observed in the case of both high-aspect-ratio wings [23,26] and low-aspect-ratio wings [24]. The wake direction (deflection angle) is constant or time dependent [23,27,29]. Similar asymmetric vortex patterns have been reported for a simple flapping wing [31–34], a wing with both heaving and flapping motion [30,35–37], and even for a wing model that can move according to the generated thrust [38–41].

In this paper, we use a simple model to show that temporal frequency reduction can cause inversion of the deflected wake pattern. The parameters are chosen such that the nondimensional parameters are set in the range of insects [42,43]. By limiting the wing kinematics, we clarify the parameter region for the nontrivial vortex transition. A previous study has reported vortex pattern transitions when flapping is abruptly stopped in the case of a two-dimensional free-flight model [44]; however, owing to the coupling between the vortex dynamics and the center-of-mass motion, the separation dynamics and the vortex dynamics in the parameter space of wing kinematics were not examined in detail. The model analyzed here is simplified considerably to focus on changes in the vortex pattern on the basis of smooth wing kinematics.

The remainder of this paper is organized as follows. Section II describes the details of the model and the numerical method. Section III presents the results. Vortex structures and the lift and drag in simple heaving motion are discussed in Sec. III A, whereas the transition of the vortex structures owing to nonperiodic wing motion is discussed in Sec. III B. Further, the Reynolds number dependence on the discovered vortex transition process is discussed in Sec. III C. Finally, Sec. IV concludes the paper.

II. MODEL

A. Wing kinematics

A heaving wing in a two-dimensional uniform flow (Fig. 1) is considered. We assume that the wing is a plate with wing chord length c and thickness $c\delta$, and that both ends are semi-circles of radius $c\delta/2$. The wing, which oscillates vertically to the uniform flow $\boldsymbol{U}_0 = (U_0, 0)$, is always parallel to $\boldsymbol{U}_0$, and the center of the wing, $\boldsymbol{X}_w$, moves perpendicular to $\boldsymbol{U}_0$: $\boldsymbol{X}_w = (0, h(t))$. The function $h(t)$ is defined as

$$h(t) = A \sin \Phi(t), \tag{1}$$

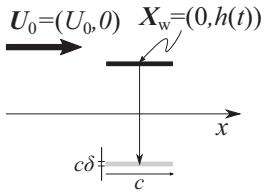

FIG. 1. Configuration of the model. A wing in a two-dimensional uniform flow oscillates perpendicular to the uniform flow. The position of the center of the wing is described by $\boldsymbol{X}_w = (0, h(t))$.

where the constant A is the oscillation amplitude and the function $\Phi(t)$ is the phase of the oscillation, which determines the details of the wing motion. When $\Phi(t) = \omega t$ (ω is the constant angular velocity), the wing motion is simple heaving. To describe the general wing kinematics, we need an infinite number of parameters. However, in this paper, the wing motion is restricted such that $\Phi(t)$ is described as follows:

$$\begin{aligned}\Phi(t) &= \Phi(t; \omega, \Delta\omega, t_1, t_2) \\ &= \phi + \omega t - (t_2 - t_1) F(t; t_1, t_2) \Delta\omega,\end{aligned} \tag{2}$$

where the constants ϕ and $\Delta\omega$ are the initial phase of oscillation and the decrement in angular frequency, respectively. The function $F(t; t_1, t_2)$ is defined as

$$\begin{aligned}F(t; t_1, t_2) &= \sigma\left(t - \frac{t_1 + t_2}{2}, \frac{4}{t_2 - t_1}\right), \\ \sigma(x, a) &= \frac{1}{2}\left(\tanh\frac{ax}{2} + 1\right),\end{aligned} \tag{3}$$

where $\sigma(x, a)$ is the sigmoid function that connects 0 and 1 smoothly around $x = 0$, i.e., $\lim_{x\to-\infty}\sigma(x, a) = 0$ and $\lim_{x\to\infty}\sigma(x, a) = 1$, with characteristic width $1/a$. Thus, the function $\Phi(t; \omega, \Delta\omega, t_1, t_2)$ shifts the phase of oscillation by $-\Delta\omega(t_2 - t_1)$; in other words, the local angular velocity, defined by $\partial\Phi/\partial t$, undergoes a temporal decrease of $-\Delta\omega$ at $t = (t_1 + t_2)/2$. The change mainly occurs in the time interval $[t_1, t_2]$ (cf. Fig. 8).

B. Numerical method of fluid motion

To numerically solve the fluid motion according to the wing motion, we use a coordinate system in which the wing is fixed. Let us define the coordinate system in the laboratory frame as O-xy and the wing-fixed coordinate system as O-XY.

The velocity and acceleration of the center of the wing in the O-xy system are $\boldsymbol{V}_w = (0, h'(t))$ and $\boldsymbol{A}_w = (0, h''(t))$, respectively. When the fluid velocity in the O-xy system is $\boldsymbol{u}$, the fluid velocity in the O-XY system, $\boldsymbol{U}$, is given by $\boldsymbol{U} = \boldsymbol{u} - \boldsymbol{V}_w$. Similarly, when the force in the O-xy system is $\boldsymbol{f}$, the force acting on the wing in the O-XY system, $\boldsymbol{F}$, is given by $\boldsymbol{F} = \boldsymbol{f} - \rho_w B \boldsymbol{A}_w$. Note that the force calculated in the O-XY system includes an artificial force proportional to the acceleration and volume of the wing; $\rho_w B \boldsymbol{A}_w$, where ρ_w and B are the density and volume (area in the two-dimensional case) of the wing, respectively. These formulae give the transformation between variables in both coordinate systems. In the following, we represent the values of all the variables in the O-xy coordinates, although the calculation was performed

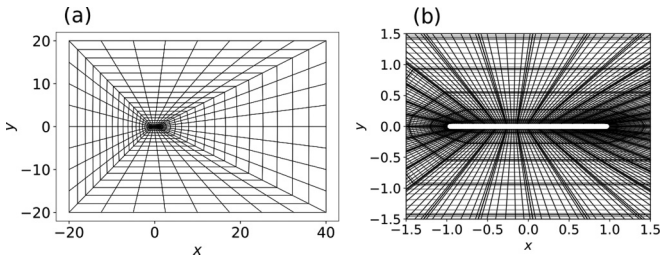

FIG. 2. (a) Subregions for the simulation domain. (b) Subregions (divided by thick lines) and the collocation points (represented by the crossing points of thin lines) near the wing.

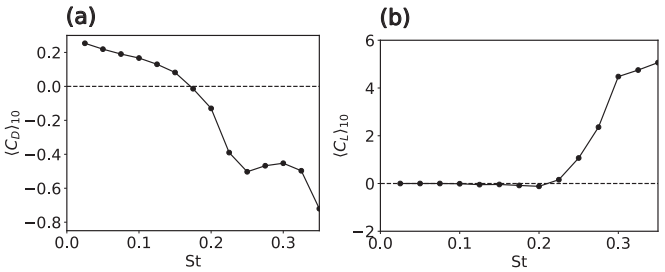

FIG. 3. $\langle C_D\rangle_{10}$ and $\langle C_L\rangle_{10}$ for $\phi=\pi$. (a) $\langle C_D\rangle_{10}$ vs St. (b) $\langle C_L\rangle_{10}$ vs St.

in the O-XY coordinates (for comparison with the calculation using the immersed boundary method in the laboratory frame, refer to the Appendix).

The fluid motion is governed by the incompressible Navier-Stokes (NS) equations:

$$\frac{\partial \boldsymbol{u}}{\partial t}+\boldsymbol{u}\cdot\nabla\boldsymbol{u}=-\frac{1}{\rho}\nabla p+\nu\nabla^2\boldsymbol{u},\quad \nabla\cdot\boldsymbol{u}=0, \tag{4}$$

where $\boldsymbol{u}=(u,v)$ is the velocity field, p is the pressure, and ν is the kinematic viscosity.

In this model, we have three nondimensional parameters: Reynolds number $\mathrm{Re}=\frac{U_0 c}{\nu}$, Strouhal number $\mathrm{St}=\frac{fA}{U_0}$ ($f=\frac{\omega}{2\pi}$), and the nondimensional amplitude $r=\frac{A}{c}$.

The fluid motion is solved using the spectral element method (SEM), which is a high-order finite element technique that combines the geometric flexibility of finite elements with the high accuracy of spectral methods. We used *Semtex* [45], an open-source SEM package that has been used in many hydrodynamic problems.

In this study, the computational domain is $[X_1,X_2]\times[Y_1,Y_2]$. The boundary condition at the outer sides of the domain is inflow with $\boldsymbol{u}=\boldsymbol{U}_0$ except for the right side ($x=X_2, Y_1\leqslant y\leqslant Y_2$), where the robust outflow condition proposed by Dong *et al.* [46] with a smoothness parameter ("δ" in their paper) of 0.1 is applied. The domain is decomposed into $N_1\times N_2$ quadrilateral subregions ("elements" in the Semtex manual) with O-type geometry; N_1 and N_2 denote the number of divisions in the azimuthal and radial directions, respectively. Each subregion contains M^2 Lagrange knot points (Fig. 2).

The parameters of the system were as follows: $U_0=1$, $\rho=1$, $c=2$, $\delta=0.05$, $A=0.6$, and $r=0.3$. For numerical simulation, we used $N_1=32$, $N_2=20$, $M=9$, $X_1=-20$, $X_2=40$, $Y_1=-20$, and $Y_2=20$. The time integration was of the second order with time step $\Delta t=1.0\times10^{-4}T$, where $T=1/f$ is the heaving period. The grid width in the subregions attached to the wing ranged from 2.13×10^{-3} to 2.83×10^{-2}. The initial state was $\boldsymbol{u}(t=0)=\boldsymbol{U}_0$. In the following, $\mathrm{Re}=200$, and we controlled St, t_1, t_2, and $\Delta\omega$ except for Sec. III C, where Re was changed.

We confirmed that the main result with the physical parameters $(\mathrm{St},\Delta\omega,t_1,t_2)=(0.275,\omega/2,7\frac{1}{3},8\frac{1}{3})$ (see Sec. III B) as well as the results with the simple heaving ($\Delta\omega=0$, $0.1\leqslant\mathrm{St}\leqslant0.3$) did not change with finer simulation parameters $(N_1,N_2,M,\Delta t)=(40,25,11,T/15000)$.

III. RESULTS

A. Simple heaving

1. Transition of vortex pattern

First, we show the results with $\Delta\omega=0$ (simple heaving) to explain the vortex patterns observed in this system. In this case, the heaving motion is periodic and the vortex patterns depend on St [23,29]. We considered the case of $\phi=\pi$ for the integration time $10T$. Figure 3 shows $\langle C_L\rangle_{10}$ and $\langle C_D\rangle_{10}$ for $0.025\leqslant\mathrm{St}\leqslant0.35$, where $\langle C_L\rangle_n$ and $\langle C_D\rangle_n$ denote the period-averaged lift and period-averaged drag, respectively, $\langle C_L\rangle_n=\frac{1}{T}\int_{(n-1)T}^{nT}C_L\,dt$, and a similar formula applies to $\langle C_D\rangle_n$.

Figure 3(a) shows that the sign of $\langle C_D\rangle_{10}$ changes at $\mathrm{St}\simeq0.175$. When St is below the critical value, the horizontal force acting on the wing is positive (drag), and a negative force (thrust) is generated above the critical value. Figure 3(b) shows the transition of $\langle C_L\rangle_{10}$ from smaller values to order-of-unity values occurring at $\mathrm{St}\simeq0.20$, i.e., a transition from a symmetric vortex pattern to an asymmetric one. A symmetric vortex pattern with drag ($\mathrm{St}=0.10$) is shown in Fig. 4(a), and an asymmetric vortex pattern, i.e., wake deflection, with thrust ($\mathrm{St}=0.275$) is shown in Fig. 4(b). The major vortex structure is generated up to $t=10T$. The asymmetric vortex pattern loses its order when $\mathrm{St}\geqslant0.325$. In this case, both the leading-edge vortex (LEV) and the trailing-edge vortex (TEV) are released from the wing to generate an irregular pattern [Fig. 4(c)]. A chaotic flow generation due to LEV-TEV interaction was analyzed in the case of the pitching and heaving wing with larger Reynolds number (1000) [37]

2. Vortex dynamics in wake deflection

The details of the asymmetric vortex pattern also depend on the initial phase ϕ; two cases, $\phi=\pi/2$ and $\phi=\pi$, were compared. In the range $\mathrm{St}\leqslant0.20$ (symmetric vortex pattern), there is no significant difference between the two cases. However, a difference is observed when $\mathrm{St}\geqslant0.20$, which suggests that the asymmetric vortex pattern depends on ϕ, though the symmetry is broken in both the cases (data not shown).

In this paper, we define the asymmetric vortex pattern for large values of $|\langle C_L\rangle_n|$ (larger than 2.0), i.e., "deflected wake" [23]. In this case, the wake deflection is clear, and the deflection angle of the asymmetric pattern α, i.e., the angle between the x axis and the line passing near the trailing edge and the separation vortices, takes a positive value. The angle depends on the initial condition; the inverted pattern

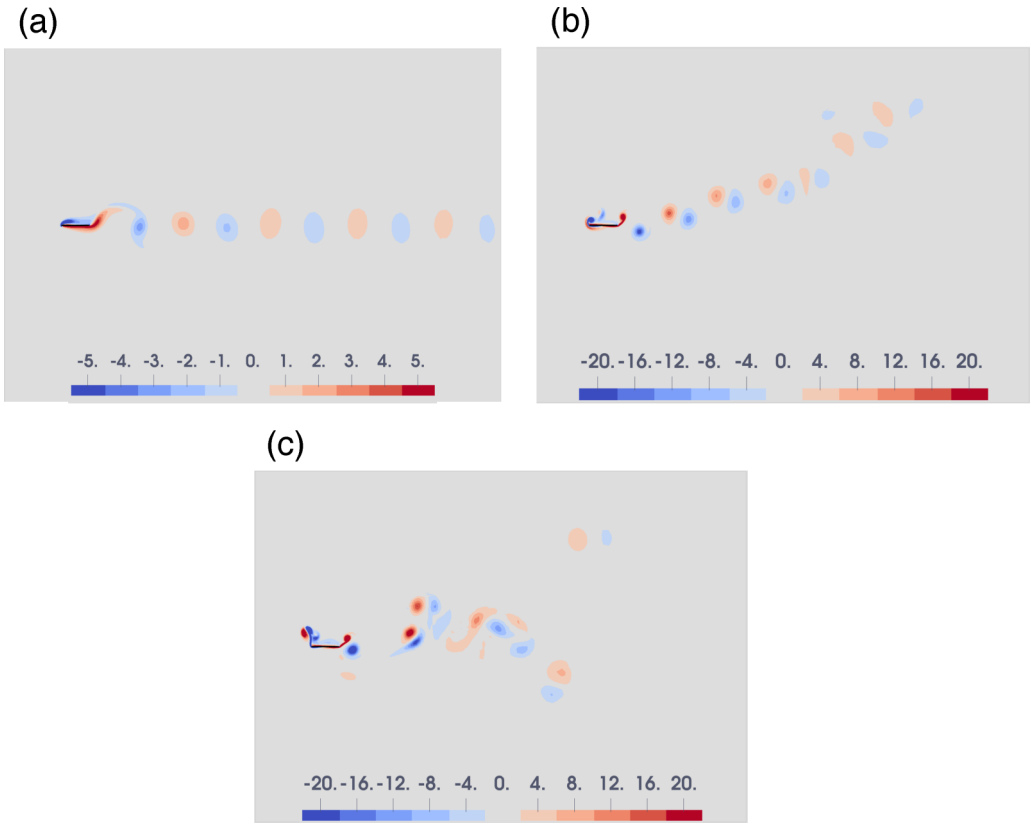

FIG. 4. Vortex pattern at $t = 10T, \phi = \pi$. The displayed region is $[-5, 30] \times [-12.5, 12.5]$. The vorticity, $\nabla \times \boldsymbol{u}$, is shown by filled contours. (a) St = 0.10. (b) St = 0.275. (c) St = 0.35.

with the deflection angle $-\alpha$ can be obtained when the initial phase is shifted by π.

We remark that this difference of $\langle C_L \rangle_n$ for the initial phase ϕ is not transient. In Fig. 5(a), $\langle C_L \rangle_n$ for $\phi = \pi/2$ and $\phi = \pi$ for St = 0.275 are shown for the number of periods, n. In the case of $\phi = \pi$, the deflection angle keeps positive (upward) from the beginning of wake formation, but the size of LEV becomes large and the wake structure changes (i.e., the distance between the vortices consisting of the dipoles becomes shorter) as n becomes large [Figs. 5(b) and 5(c)]. Then, LEV interacts with the wake via TEV, which causes an instability of the whole vortex structure to fluctuate. Such LEV-TEV interaction is also referred to in the context to a trigger to chaos in the flow around the heaving-pitching wing for larger Reynolds number [37]. On the other hand, in the case of $\phi = \pi/2$, the vortex structure is horizontal rather than deflected [Fig. 5(d)]. The line passing between positive and negative vortices waves aperiodically as it goes downstream, which causes small fluctuations of $\langle C_L \rangle_n$. Clearly, $\langle C_L \rangle_n$ depends on ϕ, and the difference is observed up to at least $100T$ [47]. Such simulations of the heaving wing suggest that the deflection angle varies with time over a long timescale (over 100 periods) [27], but the present integration time is not sufficiently long to diagnose the periodicity. It seems that such long-lasting initial phase dependence has not been reported previously.

The formation of the asymmetric vortex pattern is related to the values of $\langle C_L \rangle_n$. The interference of separation vortex generation with the vortex structure may be represented by the increment in $\langle C_L \rangle_n$, i.e., $\langle C_L \rangle_n - \langle C_L \rangle_{n-1}$ (or gradient of the graph). Figure 5 shows that the increments in $\langle C_L \rangle_n$ for $n < 7$ are larger than those for $7 < n < 40$, which suggests that the vortex structure generated before $n = 7$ is qualitatively different. This observation is in agreement with the fact that the major vortex pattern is generated up to $10T$ [Figs. 6(a) and 6(b)]. The function $\langle C_L \rangle_n$ for $n > 40$ shows fluctuations due to the stability of the deflected wake with many vortices. Hereafter, we mainly focus on the vortex structure generated until around $t = 15T$, which covers the critical number of periods determined by the lift increment. Focusing on this time range, we can omit the effect of the boundary condition because the wake structure does not reach the outer boundary, and the instability of the wake is not observed. This time range also covers the minimum period for the lift inversion discussed in Sec. III B.

The maintenance of the deflected wake is due to the following factors: (1) generation of the asymmetric vortex pattern by the TEV and (2) noninterference of the LEV with the TEV. These factors are clearly observed in Fig. 6, where the sequence of the vortex patterns near the wing is shown over one period. (See the Supplemental Material [48] for vortex dynamics generated by simple heaving wing.)

For the first factor, St is larger than those for symmetric vortex patterns, which means that the angular frequency and the heaving speed are also larger. Thus, the generated TEV has larger circulation. The interactions of the TEV with other shed vortices are stronger, and they break the symmetry of the vortex pattern with respect to the direction of uniform flow. This mechanism is reproduced by the simulation without the

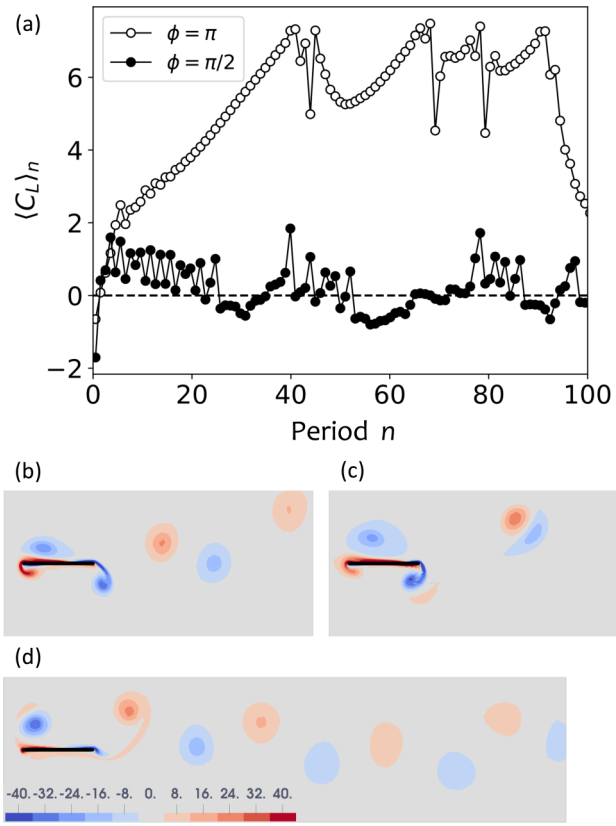

FIG. 5. (a) Plot of $(n - \frac{1}{2}, \langle C_L \rangle_n)$ for different initial phases ($\phi = \pi/2, \pi$). (b) Snapshot of the wing and vortices for $t = 10.5T$ and $\phi = \pi$. Vorticity is indicated by filled contours; the boundaries are $\nabla \times \boldsymbol{u} = \pm(4 + 8k)$ $(k = 0, 1, \ldots, 5)$. (c) Same as (b), but for $t = 40.5T$. (d) Same as (b), but for $t = 70.5T$ and $\phi = \pi/2$.

LEV, which was determined by the discrete vortex method considering the separation from the trailing edge alone [23].

For the second factor, we follow the dynamics of the LEV. Two LEVs with positive and negative signs are generated during upstroke and downstroke, respectively. We focus on the LEV with the negative sign generated during the downstroke [LV_n in Fig. 6(a)]. The LEV is connected with the leading

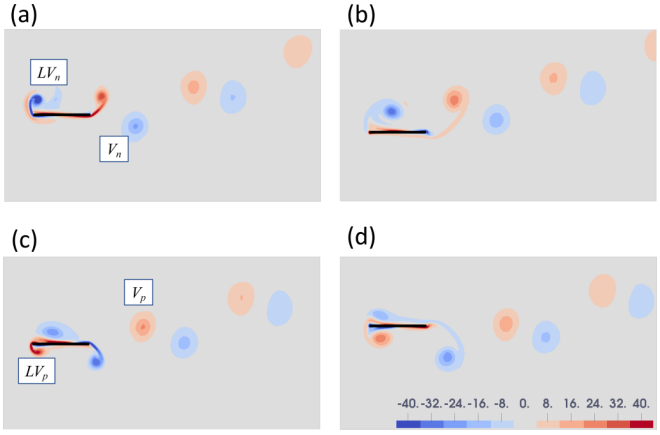

FIG. 6. Time sequences of vortex patterns for St = 0.275. (a) $t = 9.00T$. (b) $t = 9.25T$. (c) $t = 9.50T$. (d) $t = 9.75T$.

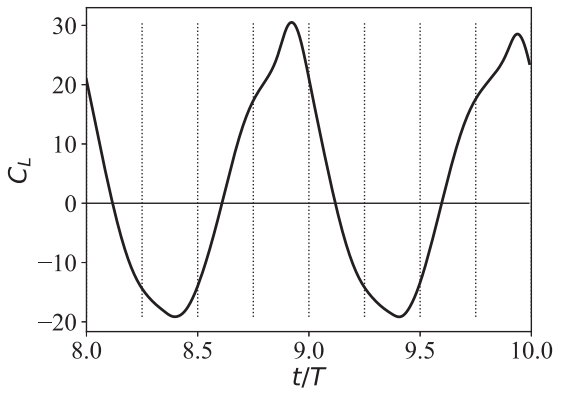

FIG. 7. C_L vs t/T for St = 0.275 ($8T \leqslant t \leqslant 10T$).

edge via a thin vortex layer [Fig. 6(b)] before it is stretched and dissipated owing to the upstroke [Figs. 6(c) and 6(d)]. However, a part of the vortex remains and merges with the separation vortex generated during the next downstroke. On the other hand, the LEV with the positive sign generated during the upstroke [LV_p in Fig. 6(c)] is stretched, and most of it is dissipated. These processes show that the LEV does not interfere with the TEV dynamics significantly.

Neither dissipation nor trapping of LEVs occur when St is much larger (St $\geqslant 0.35$); the LEVs also detach from the wing and disturb the patterns due to the TEVs, and the entire vortex pattern becomes irregular [Fig. 6(c)]. In other words, the suppression of LEV-TEV interference gives an important condition for generation of the deflected wake. Controlling the LEV-TEV interference might enable us to realize a change in the vortex structure.

The instantaneous lift coefficient is shown in Fig. 7. Asymmetric lift generation is clearly observed. In the interval $9T < t < 10T$, positive lift is generated when $t < 9.12T$ and $9.60T < t$, whereas negative lift is generated when $9.12T < t < 9.60T$. As $\phi = \pi$, the downstroke is observed when $t < 9.25T$ and $9.75T < t$, which corresponds to the interval of positive lift in an approximate sense. The vortex dynamics in the positive lift generation is shown in Figs. 6(a) and 6(d) [the pattern in Fig. 6(d) is nearly the same as the pattern at $t = 8.75T$]. In this sequence, the free vortex with a negative sign near the TEV [V_n in Fig. 6(a)], which was detached from the trailing edge, remains near the trailing edge; thus, the lift generation is enhanced. On the other hand, the negative lift generation is relatively weak because the free vortex with a positive sign near the TEV [V_p in Fig. 6(c)] is not as close to the trailing edge as in the downstroke. The effect of the free vortex on the lift generation is reminiscent of the wake capture in insect flight [49]. The asymmetric lift generation results in a nonzero value of the total lift.

B. Temporal reduction of heaving frequency

In this section, we demonstrate that an inversion of the vortex pattern associated with the lift sign can be triggered by a temporal reduction in the heaving frequency when St = 0.275, $\phi = \pi$, and $\Delta\omega = \omega/2$. Figure 8 shows the local angular frequency $\partial\Phi/\partial t$ and nondimensional heaving motion $h(t)/A$ for $(t_1/T, (t_2 - t_1)/T) = (7\frac{1}{3}, 1)$. In this case,

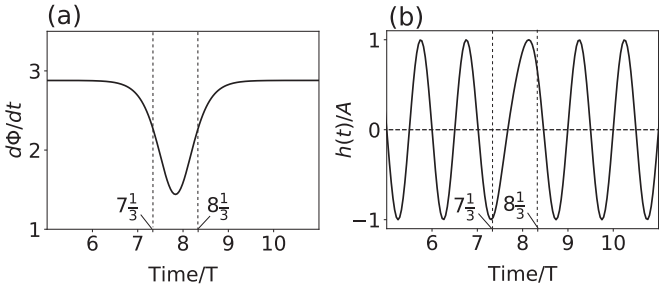

FIG. 8. Wing kinematics for $\Delta\omega = \omega/2, t_1 = 7\frac{1}{3}T, t_2 = 8\frac{1}{3}T$. (a) $d\Phi/dt$ (b) $h(t)/A$.

the frequency reduction is apparent in the eighth flapping, while the change is smooth according to the definition of the class of the wing motion.

Figure 9 shows a series of $\langle C_D\rangle_n$ and $\langle C_L\rangle_n$ for two typical cases, $t_1/T = 7$ and $7\frac{1}{3}$, to demonstrate how the inversion depends on (t_1, t_2). In both cases, a strong disturbance due to the wing motion causes a significant change in the period-averaged values. The results for the case $t_1/T = 7$ are shown in Figs. 9(a) and 9(c). In this case, regardless of the value of t_2, the values of $\langle C_L\rangle_n$ and $\langle C_D\rangle_n$ in the last period did not change significantly. In particular, the sign of $\langle C_L\rangle_n$ did not change for all values of t_2 in $0.4 \leqslant (t_2 - t_1)/T \leqslant 1.6$. In other words, the disturbances when $t_1/T = 7$ did not change the eventual vortex structures.

The results for the case $t_1/T = 7\frac{1}{3}$, in which t_1 is slightly different value from that of the above-mentioned case, are shown in Figs. 9(b) and 9(d). It is clear that the sign of the lift is inverted for several values of t_2 with decreasing values in the latter periods. Figure 10(a) shows the detailed values of $\langle C_L\rangle_{15}$ for $t_1/T = 7\frac{1}{3}$. A wide range of values of $(t_2 - t_1)/T$ gives greater negative values [e.g., $\langle C_L\rangle_{15} < -1$

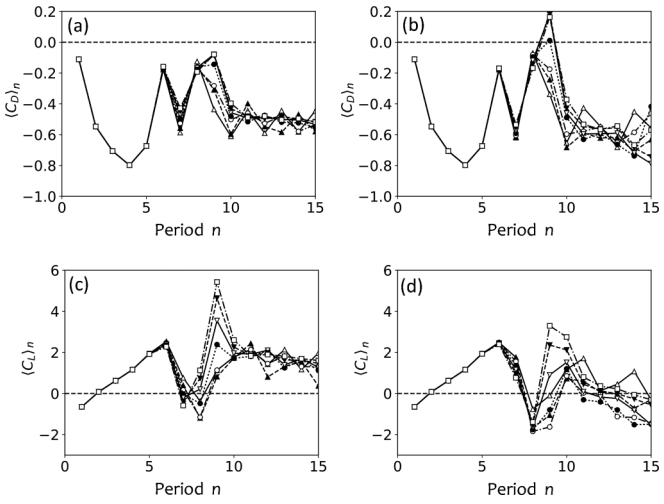

FIG. 9. (a) $\langle C_D\rangle_n$ vs n (n is the period) for $t_1/T = 7.0$. The open triangle (△), filled triangle (▲), open circle (○), filled circle (●), open inverted triangle (▽), closed inverted triangle (▼), and open square (□) indicate $(t_2 - t_1)/T = 0.4, 0.6, 0.8, 1.0, 1.2, 1.4, 1.6$, respectively. (b) Same as panel (a), but $t_1/T = 7\frac{1}{3}$. (c) $\langle C_L\rangle_n$ vs n for $t_1/T = 7.0$. (d) Same as panel (c), but $t_1/T = 7\frac{1}{3}$.

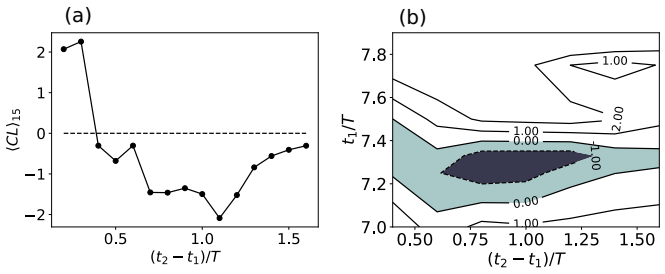

FIG. 10. (a) $\langle C_L\rangle_{15}$ vs $(t_2 - t_1)/T$ for $t_1/T = 7\frac{1}{3}$. (b) Contour of $\langle C_L\rangle_{15}$ for sets of $(t_1/T, (t_2 - t_1)/T)$, where $t_1/T \in \{7, 7\frac{1}{4}, 7\frac{1}{3}, 7\frac{1}{2}, 7\frac{3}{4}, 7\frac{5}{6}\}$ and $(t_2 - t_1)/T \in \{0.4, 0.6, 0.8, 1.0, 1.2, 1.4, 1.6\}$. The region $\langle C_L\rangle_{15} < 0$ is shaded.

for $0.7 \leqslant (t_2 - t_1)/T \leqslant 1.2$)]. These results suggest that the lift inversion is robust for the values of $(t_2 - t_1)$ around $(t_2 - t_1)/T = 1.0$.

The result of a parametric study on the lift inversion is shown in Fig. 10, where $\langle C_L\rangle_{15}$ was used. In Fig. 10(b) the contour of $\langle C_L\rangle_{15}$, which was used as a characteristic variable of the inversion, is shown for sets of $(t_1/T, (t_2 - t_1)/T)$. We can see that the range around $(t_1/T, (t_2 - t_1)/T) = (7\frac{1}{3}, 1)$ gives negative values [shaded region in Fig. 10(b)] corresponding to the lift inversion. We remark that the time interval of reduced frequency $t_2 - t_1$ considered here is less than $1.5T$, which implies that the phenomena discussed here is due to unsteady (nonperiodic) dynamics of wing and the flow.

Next, the robustness to the characteristic start time of the frequency reduction, t_1, is examined. Figure 11 shows $\langle C_L\rangle_n$ as a function of n. We fixed $(t_2 - t_1)/T = 1$. Four cases for $t_1/T = 4\frac{1}{3}$, $7\frac{1}{3}$, $10\frac{1}{3}$, and $13\frac{1}{3}$ and a case of no frequency reduction ($t_1 \to \infty$) are shown to examine the relationship between the vortex structure at the beginning of the reduction and the final result. Note that the phase of the frequency reduction was fixed because it is important for the inversion, as shown in Fig. 10(b). Figure 11 shows that the case

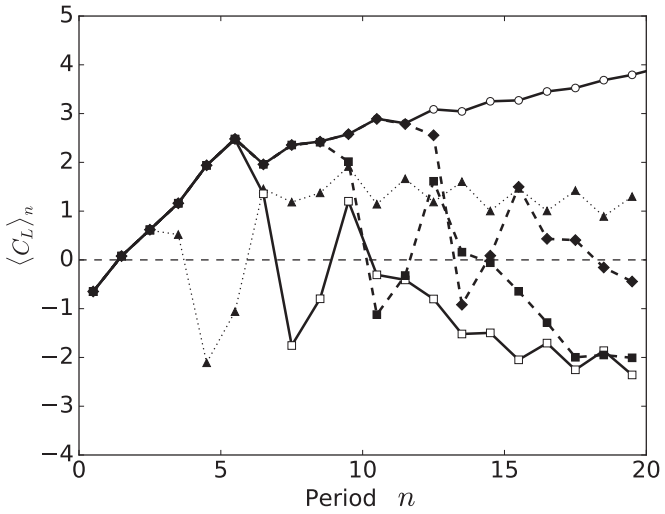

FIG. 11. $\langle C_L\rangle_n$ vs n. The open circles indicate the case of no maneuvering ($\Delta\omega = 0$). The filled triangles (▲), open squares (□), filled squares (■), and diamonds (♦) indicate $t_1/T = 4\frac{1}{3}, 7\frac{1}{3}, 10\frac{1}{3}$ and $13\frac{1}{3}$, respectively.

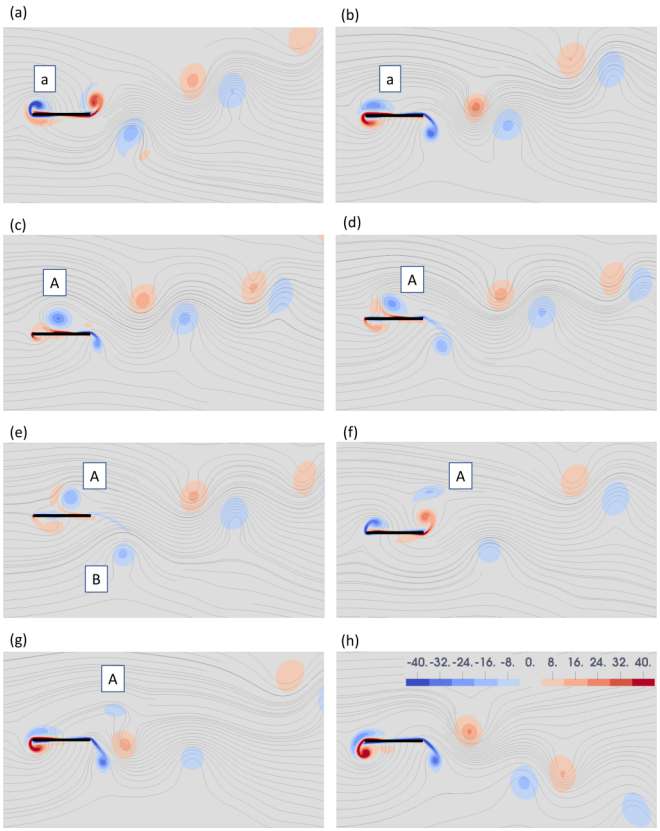

FIG. 12. Vortex patterns during temporal reduction of the local angular frequency ($t_1/T = 7\frac{1}{3}, t_2 - t_1 = T$). Curves indicate streamlines. (a) $t = 6.0T$. (b) $t = 6.5T$. (c) $t = 7.5T$. (d) $t = 7.75T$. (e) $t = 8.0T$. (f) $t = 8.5T$. (g) $t = 9.0T$. (h) $t = 14.0T$.

$t_1/T = 4\frac{1}{3}$ did not reach the final inversion, which suggests that the vortex structure generated up to this time is not sufficiently "mature" to accept the transition mechanism discussed below. The time series of $\langle C_L \rangle_n$ for $t_1/T = 7\frac{1}{3}$, $10\frac{1}{3}$, $13\frac{1}{3}$ are rather universal. The lift sign changes once to negative during the temporal frequency reduction and then changes to positive for one or two periods; finally, decreasing negative values are observed. This result suggests that the process of the transition in the vortex structure has a universality property and the temporal frequency reduction strategy for the lift inversion requires a "matured" vortex structure that contains several coherent vortices. In the following, we consider the case $t_1/T = 7\frac{1}{3}$, $(t_2 - t_1)/T = 1$ as a typical example. We note that similar inversion process is observed when $0.26 \leqslant \mathrm{St} \leqslant 0.28$ while keeping other parameters the same.

The vortex dynamics during the reduction is shown in Fig. 12. (See the Supplemental Material [48] for vortex dynamics generated by heaving wing with temporal frequency reduction.) As explained in Sec. III A, the LEVs are dissipated or trapped near the leading edge in the simple heaving motion, which also occurs before the reduction starts ["a" in Figs. 12(a) and 12(b)]. However, the temporal frequency reduction weakens the stretching or dissipation process of the LEVs. Because of slower upward motion of the wing in this process, the LEV above the wing did not stretch considerably, resulting in its survival ["A" in Fig. 12(c)]. Because this vortex is generated before the frequency reduction, the magnitude of the vorticity is close to the corresponding vortex in simple heaving [Figs. 5(b) and 5(c)], although the detailed shape depends on the wake structure. Figures 12(c)–12(f) show the dynamics during the frequency reduction interval. The streamlines indicate that the flow around the LEV "A," which is detached from the leading edge, is rightward. The time interval of the frequency reduction is sufficient to transfer the LEV "A" to the trailing edge, and the LEV reaches without significant distortion or dissipation. The negative sign of the LEV induces stronger local velocity near the trailing edge. As a result, the LEV shifts the position of the TEV generated in this interval ["B" in Fig. 12(e)]. Moreover, the LEV "A" remains near the trailing edge during the next period to induce a backward flow so that the vortices near the trailing edge are not advected excessively. Then a dipole vortex moving in an obliquely downward direction is generated [Figs. 12(f) and 12(g)]. The arrangements of the vortices significantly change the position of the subsequently generated coherent vortices to finally invert the vortex pattern [Fig. 12(h)]. The vortex patterns in Figs. 12(a) and 12(h) are roughly symmetric with respect to a horizontal line [note that the phase of the wing oscillation shifted by $-\Delta\omega(t_2 - t_1) = -\pi$].

It should be remarked that the unsteady wing-vortex interaction during the lift inversion matches the successful parameters of (t_1, t_2). Actually, Fig. 10(b) suggests that $(t_2 - t_1)/T$ should be around unity, and the phase of t_1 is around 1/3 (of the period). The former corresponds to the order of time to transfer LEV along the wing cord, and the latter is a condition for the wing to upward slowly during frequency reduction period.

The essential part of this transition dynamics can be extracted from the time-expanded images shown in Fig. 13. Figure 13(a) is generated by stacking the line vorticity distribution $c/4$ above the wing; a horizontal cross section of the figure shows the spatial vorticity distribution, and a vertical cross section shows the time series of the vorticity at a particular point. In the time interval "A," two lines per one period are shown on the right (downstream). These lines indicate positive and negative vortices generated to form the deflected wake with a positive deflection angle [corresponding to Fig. 12(a)]. The LEV transfer above the wing is indicated by the region "V" for the time interval $[7T, 8T]$. The transferred LEV interacts with the TEV to change the deflection angle. After the interaction, one of the lines, corresponding to negative vortices, disappear because the deflection angle is inverted.

Figure 13(b) is generated similarly to Fig. 13(a), but for the line vorticity distribution $c/4$ *below* the wing. The vortex pattern before the frequency reduction is similar to that in Fig. 13(a) after the frequency reduction with the inverted sign, suggesting that the deflection pattern is inverted during the process. Similarly, the vortex pattern in Fig. 13(a) during the period "A" is similar to that in Fig. 13(b) during the period *after* the frequency reduction with the inverted sign (indicated by "B"). These images clearly show the inversion dynamics, especially for the effect of LEV transfer.

Furthermore, the vortex pattern indicated by "v′" shows an irregular transfer of a part of the LEV without temporal

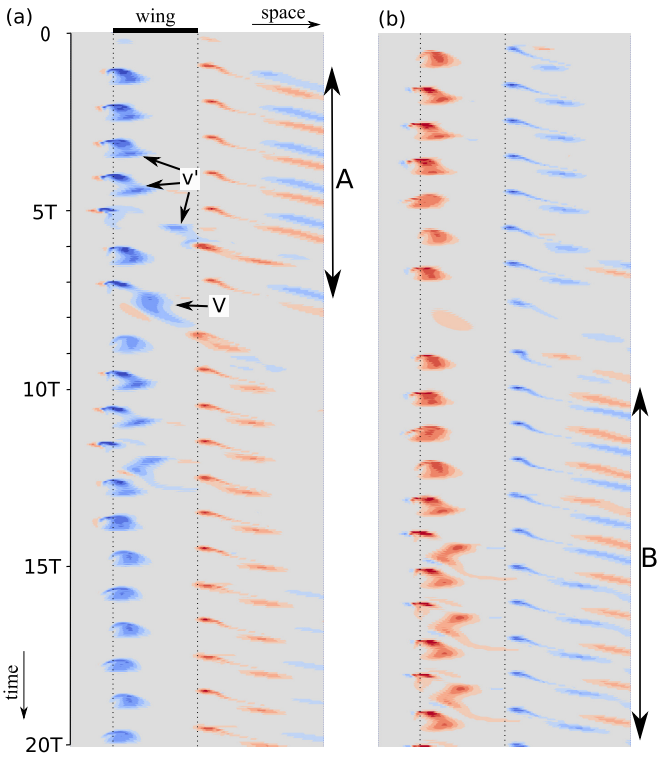

FIG. 13. Time expanded image for $t_1/T = 7\frac{1}{3}, t_2 - t_1 = T$. This image was generated by stacking the horizontal line distribution of vorticity from top to bottom, for the interval $0 \leqslant t \leqslant 20T$, $-2 \leqslant x \leqslant 4$. The legend is the same as that for Fig. 6. (a) Image for the horizontal line $c/4$ above the wing. (b) Image for the horizontal line $c/4$ below the wing.

frequency reduction. Although the entire vortex pattern is disturbed by such an irregular vortex transfer that is observed sometimes, it does not change significantly (cf. Fig. 5).

C. Discussion: The Reynolds number dependency

In this subsection, we discuss the Reynolds number dependence on the transitions of the vortex structures.

First, the transition behaviors of $\langle C_D\rangle_n$ and $\langle C_L\rangle_n$ for different St values are determined for the case Re = 150, $\phi = \pi$. Figure 14 shows the result, together with the case Re = 200, which suggests that the vortex transition for different St values does not change significantly in this interval, though a slight increment in the value of $\langle C_D\rangle$ is observed for Re = 150.

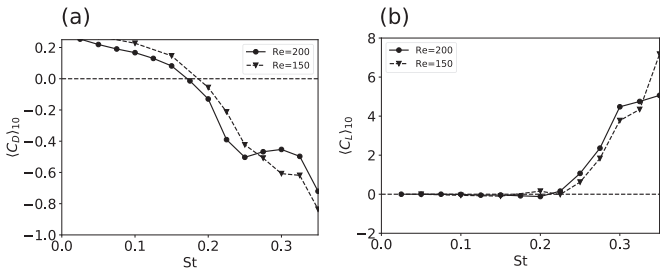

FIG. 14. (a) Reynolds number dependence on the transitions of $\langle C_D\rangle_{10}$. (b) Same as panel (a) but for $\langle C_L\rangle_{10}$.

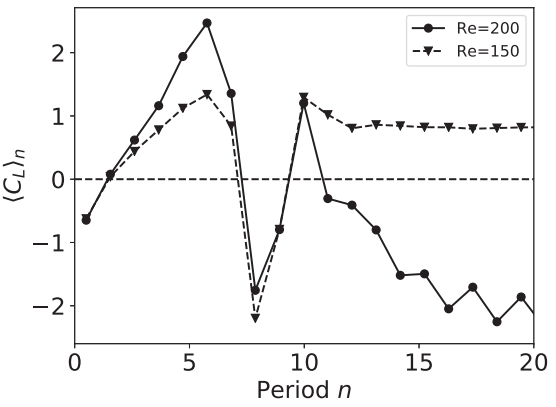

FIG. 15. $\langle C_L\rangle_n$ vs n for the cases Re = 150, 200, where $t_1/T = 7\frac{1}{3}$ and $t_2 - t_1 = T$.

However, in particular, the behavior at St = 0.275, which has been discussed in detail in Sec. III A 1, is the same; i.e., thrust is generated and the asymmetric vortex pattern is observed. The transition behaviors of the lift and the vortex structures for the temporal frequency reduction were compared for the typical case: $t_1/T = 7\frac{1}{3}$, $(t_2 - t_1)/T = 1$. Figure 15 shows the result; clearly, the lift inversion fails when Re = 150.

The difference is attributed to the large dissipation. A long-time simulation of simple heaving shows that $\langle C_L\rangle_n$ attains a plateau $t > 90T$ for the case Re = 150 (data not shown); by contrast, for the case Re = 200, $t \simeq 50T$ (Fig. 5). Moreover, the initial increase rate of $\langle C_L\rangle_n$ for Re = 150 is smaller than that for Re = 200. Because the number of vortices in the vortex structures at a particular time does not depend on Re, the low increase rate is attributed to the large dissipation. In this case, the LEV is transferred as in the case of Re = 200, but there is no rearrangement of the TEV that leads to the inversion of the lift or the vortex structure. We performed a similar analysis for the cases Re = 170 and Re = 180, and we found that the critical Reynolds number seems to lie between Re = 170 and Re = 180 (data not shown).

IV. CONCLUDING REMARKS

In this paper, we studied the inversion of the lift and the asymmetric vortex pattern of a heaving wing in a uniform flow under a temporal reduction of the angular frequency. In a parameter range, it is possible to invert the vortex pattern and the lift sign. During the inversion process, the LEV plays an important role. Without the temporal reduction of the local angular frequency, the LEV dissipates or remains near the leading edge, and it does not contribute to the vortex generation at the trailing edge significantly. However, during the temporal reduction of the local angular frequency, the LEV is advected to the trailing edge to enhance the local flow, which triggers the inversion process initiated by the position shift of the generated TEV.

We demonstrated that it is possible to control the vortex structure via the wing motion, but such control is not straightforward even in our simple configuration. Previously considered examples of lift generation based on vortex generation include wake capture [49] and the symmetry-breaking

mechanism of symmetric flapping models [50,51]. However, the mechanism presented here is used to change the qualitative vortex structure, which is different from the above-mentioned mechanisms.

Efficient usage of the LEV-TEV interference can lead to vortex pattern inversion. As discussed in Sec. III A, suppression of the LEV-TEV interference is required to maintain the deflected wake under regular flapping. Such interference might be exploited for lift vector control in the future.

It is interesting to note that the Strouhal number in the flight and swimming of many animals lies in the range of 0.2–0.4 [43], and the authors suggest that the vortex pattern generated in this range is a key underlying factor. In this region, the LEV is shed as the downstroke ends, which is in agreement with our result that the LEV transfer causes the vortex pattern change. Our results suggest that such LEV shedding behavior might be useful not only for maintaining flapping flight but also for maneuverability. Although our results are restricted to the transition of the vortex dynamics owing to change of the wing motion, we believe that they will facilitate a deeper understanding of the maneuverability of flying animals.

ACKNOWLEDGMENT

This work was partially supported by JSPS KAKENHI Grant No. JP16H04303.

APPENDIX: VALIDATION

The validity of the simulation code and the algorithm for the transformation between the laboratory frame (O-xy) and the wing-fixed frame (O-XY) was verified by comparing the lift acting on the oscillating wing in a uniform flow. We compared the SEM code with the code of the immersed boundary (IB) method, which is a variant used by Yokoyama *et al.* [16]. In the calculation of the IB method, the computational domain was $[-10, 30] \times [-5, 5]$, which was represented by 1024×256 modes corresponding to the regular intervals. The time step for the IB method was 1.6×10^{-5}. The wing chord was represented by 64 grid points, corresponding to $c = 2.5$. We compared our SEM approach with the IB approach for the case $\mathrm{Re} = 200$, $\mathrm{St} = 0.15$, $r = 0.2$. Figure 16 shows the lift coefficient C_L calculated by both methods. The time series are nearly identical, especially for the case $\delta = 0.01$.

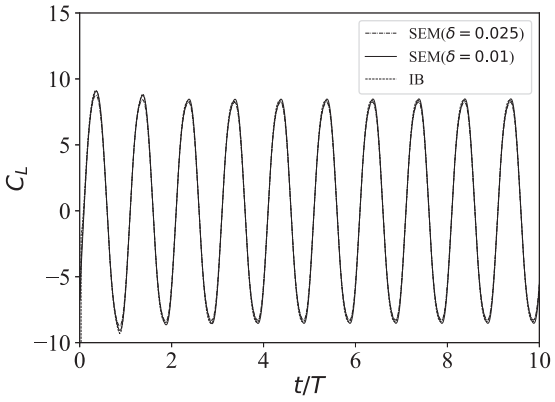

FIG. 16. Time series of the lift on the oscillating wing in a uniform flow. The calculation methods are SEM ($\delta = 0.025, 0.01$) and IB.

[1] D. D. Chin and D. Lentink, J. Exp. Biol. **219**, 920 (2016).
[2] C. P. Ellington, Philos. Trans. R. Soc. London B **305**, 79 (1984).
[3] S. P. Sane, J. Exp. Biol. **206**, 4191 (2003).
[4] Z. J. Wang, Annu. Rev. Fluid Mech. **37**, 183 (2005).
[5] C. R. Betts and R. J. Wootton, J. Exp. Biol. **138**, 271 (1988).
[6] R. Dudley, *The Biomechanics of Insect Flight: Form, Function, Evolution* (Princeton University Press, Princeton, 2000).
[7] R. B. Srygley and A. L. R. Thomas, Nature (London) **420**, 660 (2002).
[8] T. Lin, L. Zheng, T. Hedrick, and R. Mittal, Bioinspir. Biomim. **7**, 044002 (2012).
[9] T. L. Hedrick, J. R. Usherwood, and A. A. Biewener, J. Exp. Biol. **210**, 1912 (2007).
[10] R. Ramamurti and W. C. Sandberg, J. Exp. Biol. **210**, 881 (2007).
[11] Y.-H. J. Fei and J.-T. Yang, Phys. Rev. E **93**, 033124 (2016).
[12] M. Sun, Fluid Dyn. Res. **37**, 21 (2005).
[13] G. K. Taylor and R. Bikowski, J. R. Society Interface **2**, 197 (2005).
[14] I. Faruque and J. S. Humbert, J. Theor. Biol. **264**, 538 (2010).
[15] K. Senda, T. Obara, M. Kitamura, T. Nishikata, N. Hirai, M. Iima, and N. Yokoyama, Robot. Auton. Syst. **60**, 670 (2012).
[16] N. Yokoyama, K. Senda, M. Iima, and N. Hirai, Phys. Fluids **25**, 021902 (2013).
[17] T. L. Hedrick, J. Exp. Biol. **214**, 4073 (2011).
[18] N. Gao, H. Aono, and H. Liu, J. Theor. Biol. **270**, 98 (2011).
[19] S. Taneda and H. Honji, J. Phys. Soc. Jpn. **30**, 262 (1971).
[20] R. F. Huang, J. Y. Wu, J. H. Jeng, and R. C. Chen, J. Fluid Mech. **441**, 265 (2001).
[21] M. J. Ringuette, M. Milano, and M. Gharib, J. Fluid Mech. **581**, 453 (2007).
[22] K. Taira and T. Colonius, J. Fluid Mech. **623**, 187 (2009).
[23] K. D. Jones, C. M. Dohring, and M. F. Platzer, AIAA J. **36**, 1240 (1998).
[24] K. D. von Ellenrieder, K. Parker, and J. Soria, Visualization of a three dimensional heaving aerofoil foil, in *Proceeding of 14th Australasian Fluid Mechanics Conference*, edited by B. B. Dally (Casual Productions Pty. Ltd., 2001), pp. 151–154.
[25] G. C. Lewin and H. Haj-Hariri, J. Fluid Mech. **492**, 339 (2003).
[26] K. D. von Ellenrieder and S. Pothos, Exp. Fluids **44**, 733 (2007).
[27] S. Heathcote and I. Gursul, Phys. Fluids **19**, 027104 (2007).
[28] K. B. Lua, T. T. Lim, K. S. Yeo, and G. Y. Oo, AIAA J. **45**, 1571 (2007).
[29] K. D. Jones and M. F. Platzer, Exp. Fluids **46**, 799 (2009).
[30] S. Michelin and S. G. L. Smith, Phys. Fluids **21**, 071902 (2009).

[31] S. E. Spagnolie, L. Moret, M. J. Shelley, and J. Zhang, Phys. Fluids **22**, 041903 (2010).
[32] T. Schnipper, A. Andersen, and T. Bohr, J. Fluid Mech. **633**, 411 (2009).
[33] R. Godoy-Diana, C. Marais, J.-L. Aider, and J. E. Wesfreid, J. Fluid Mech. **622**, 23 (2009).
[34] R. Godoy-Diana, J.-L. Aider, and J. E. Wesfreid, Phys. Rev. E **77**, 016308 (2008).
[35] F. T. Muijres and D. Lentink, Exp. Fluids **43**, 665 (2007).
[36] K. D. V. Ellenrieder, K. Parker, and J. Soria, J. Fluid Mech. **490**, 129 (2003).
[37] C. Bose and S. Sarkar, Phys. Fluids **30**, 047101 (2018).
[38] N. Vandenberghe, S. Childress, and J. Zhang, Phys. Fluids **18**, 014102 (2006).
[39] S. Alben and M. Shelley, Proc. Natl. Acad. Sci. USA **102**, 11163 (2005).
[40] J. Zhang, N.-S. Liu, and X.-Y. Lu, J. Fluid Mech. **659**, 43 (2010).
[41] M. J. Shelley and J. Zhang, Annu. Rev. Fluid Mech. **43**, 449 (2011).
[42] K. Sato, Y. Watanuki, A. Takahashi, P. J. Miller, H. Tanaka, R. Kawabe, P. J. Ponganis, Y. Handrich, T. Akamatsu, Y. Watanabe, Y. Mitani, D. P. Costa, C.-A. Bost, K. Aoki, M. Amano, P. Trathan, A. Shapiro, and Y. Naito, Proc. R. Soc. London B **274**, 471 (2007).
[43] G. K. Taylor, R. L. Nudds, and A. L. R. Thomas, Nature (London) **425**, 707 (2003).
[44] M. Iima, N. Yokoyama, N. Hirai, and K. Senda, Adv. Sci. Technol. **84**, 59 (2013).
[45] H. Blackburn and S. Sherwin, J. Comput. Phys. **197**, 759 (2004).
[46] S. Dong, G. Karniadakis, and C. Chryssostomidis, J. Comput. Phys. **261**, 83 (2014).
[47] We remark that C_L is defined by using U as the typical velocity, while the wing speed includes the effect of heaving motion. If we take the typical velocity $\max\sqrt{U^2+|\boldsymbol{V}_w|^2} = \sqrt{U^2+(A\omega)^2} = U\sqrt{1+(2\pi \mathrm{St})^2} \simeq 2.00U$, C_L is reduced approximately $1/4$.
[48] See Supplemental Material at http://link.aps.org/supplemental/10.1103/PhysRevE.99.043110 for vortex patterns with simple heaving (Re200SimpleHeaving.mp4) and those with temporal reduction of heaving frequency (Re200Maneuver.mp4).
[49] M. H. Dickinson, F.-O. Lehmann, and S. P. Sane, Science **284**, 1954 (1999).
[50] M. Iima and T. Yanagita, J. Phys. Soc. Jpn. **70**, 5 (2001).
[51] K. Ota, K. Suzuki, and T. Inamuro, Fluid Dyn. Res. **44**, 045504 (2012).